Journal of Superconductivity and Novel Magnetism
https://doi.org/10.1007/s10948-021-05954-3

ORIGINAL PAPER

Interplay of Magnetic and Superconducting Subsystems in Ho-Doped YBCO

D. M. Gokhfeld[1,2] · S. V. Semenov[1,2] · K. Yu. Terentyev[1] · I. S. Yakimov[2] · D. A. Balaev[1,2]

Received: 31 May 2021 / Accepted: 19 June 2021
© The Author(s), under exclusive licence to Springer Science+Business Media, LLC, part of Springer Nature 2021

Abstract
Superconducting and paramagnetic contributions to the magnetization of polycrystalline $Y_{1-x}Ho_xBa_2Cu_3O_{7-\delta}$ samples were investigated. The superconductivity is responsible for a partial screening of magnetic ions from an external magnetic field and for a possible sinking of antiferromagnetic correlations between these ions. Magnetic moments of Ho ions influence on a peak effect induced by the order–disorder transition of the Abrikosov vortex lattice. The critical current density and the critical temperature of YBCO are not changed by the Ho doping.

Keywords Peak effect · Bulk superconductors · Critical current · Pinning · X-ray diffraction · YBCO · Doping · Paramagnetic magnetization

1 Introduction

Magnetization data of high-T_c superconductors in the temperature range below the critical temperature T_c contain information about a vortex system, phase homogeneity, microstructure, and critical current density. The $YBa_2Cu_3O_{7-\delta}$ superconductor (YBCO) also has some weak contributions to the magnetization (Pauli paramagnetism, Van Vleck paramagnetism, etc.) [1, 2]. A significant magnetic contribution, which is comparable with a superconducting magnetization, occurs in YBCO doped by rare-earth elements with a strong magnetic moment (RE) [3–7].

Paramagnetic impurities in YBCO are expected to suppress superconductivity in local surrounding regions [8, 9] that leads to both a desired enhancement of pinning and an unwanted decrease of T_c. However, it was observed that the substitution of rare-earth elements (RE) in the Y sites of YBCO has insignificant effect on T_c [3]. Reports about RE doping influence on the critical current density in YBCO are contradictive [3, 5–7]. It should be noted that the solid state method may require different optimal synthesis temperatures for various RE substituted YBCO [10, 11]. The same conditions for different samples may result in diverse sizes of granules and in variations of critical currents.

Holmium ions have the maximal magnetic moment among other RE. The atom radii of Y (1.80 Å) and Ho (1.75 Å) are almost identical. This allows us to investigate an interaction of magnetic and superconducting subsystem in Ho-doped YBCO, disregarding the crystal lattice distortions. The article is organized as follows: the experimental techniques used are outlined in Sect. 2, experimental results are described in Sect. 3, and Sect. 4 presents the analysis of paramagnetic and superconducting contributions to the magnetization and discussion.

2 Experimental Methods

$Y_{1-x}Ho_xBa_2Cu_3O_{7-\delta}$ samples were prepared using the solid-state synthesis from Y_2O_3, Ho_2O_3, $BaCO_3$, and CuO powders. Heat treating at 910 °C during 10 h with intermediate grinding and mixing was repeated 5 times. The samples are denoted as #1, #2, and #3 for $x = 0.02$, 0.11, and 0.25 (see Table 1). For the used concentrations, an averaged distance between the doping atoms in *ab* planes is equal to integer numbers (7, 3, and 2) of the lattice constant [5, 12].

X-ray powder diffraction (XRD) data were obtained using XRD-7000S Shimadzu diffractometer (CuKα radiation). The 2θ angle ranged from 5 to 70° with a step of 0.02°. Scanning

✉ D. M. Gokhfeld
gokhfeld@iph.krasn.ru

[1] Kirensky Institute of Physics, Federal Research Center KSC SB RAS, Krasnoyarsk 660036, Russia

[2] Siberian Federal University, Krasnoyarsk 660041, Russia

Published online: 09 July 2021

Table 1 Characterization of samples

	Parameter	#1 $x=0.02$	#2 $x=0.11$	#3 $x=0.25$
XRD	Cell parameter a, Å	3.88494	3.88546	3.88702
	Cell parameter b, Å	3.82301	3.82347	3.82448
	Cell parameter c, Å	11.67992	11.67817	11.68072
	Cell volume, Å^3	173.47	173.49	173.64
	Mass fraction of $Y_{1-x}Ho_xBa_2Cu_3O_{7-\delta}$, %	96.55	97.15	97.00
	Mass fraction of Y_2BaCuO_5, %	1.37	0.87	0.80
	Mass fraction of $Ba_{0.978}CuO_{2.069}$, %	2.07	1.98	2.20
Magnetization	Critical temperature T_c, K	93.1 ± 0.4	92.6 ± 0.8	92.9 ± 0.4
	Curie–Weiss temperature Θ, K	−14 ± 3	−12 ± 1	−19 ± 1
	Curie–Weiss constant C, K	0.04	0.17	0.44
	Critical current density J_c at 4.2 K, 10^6 A cm^{-2}	11.9	11.4	10.5
	Average size of granules d, μm	2.4	3.0	3.6
	Magnetic field of the pinning force maximum at 60 K, T	5.7	4.9	4.1

electron microscopy (SEM) and energy-dispersive spectrometry (EDS) investigations of the synthesized samples were carried out using Hitachi TM 3000 microscope. Temperature dependences of the resistivity ρ(*T*) were measured by the four-probe method using the transport current of 1 mA. Magnetic measurements were performed using Quantum Design PPMS-9 T and Lakeshore VSM 8604 vibrating sample magnetometers. SEM and magnetic measurements were carried out at the Krasnoyarsk Regional Center of Research Equipment, Federal Research Center "Krasnoyarsk Science Center SB RAS".

3 Experimental Results

Figure 1 shows X-ray diffraction patterns of the synthesized samples. All the patterns have identical positions of peaks. All the peaks are seen to correspond to the peaks in a reference pattern of the orthorhombic $YBa_2Cu_3O_{7-\delta}$ material (PDF2 ICDD #79–882). The composition of the samples and cell parameters was specified with using the Rietveld method (Table 1). Real compositions were verified to comply with the nominal ones. Other phases ($Ba_{0.978}CuO_{2.069}$, Y_2BaCuO_5) are found in minor quantities, less than 3.5% in total. The linear dependence of the a, b, and c parameters on x indicates that Ho is completely dissolved in the $Y_{1-x}Ho_xBa_2Cu_3O_{7-\delta}$ compound. Distortions of the crystal lattice due to the substitution of Ho for Y in $Y_{1-x}Ho_xBa_2Cu_3O_{7-\delta}$ are insignificant, e.g., the parameter b grows only on 0.038% as x increases from 0.02 to 0.25.

SEM images of the samples are shown in Fig. 2a–c. The samples have a disordered granular structure. For all the samples, the granule sizes are distributed from 1 to 10 μm; the average granule size is about 3 μm.

Figure 2d shows a typical EDS image of the sample with $x = 0.25$. Analysis of the elemental composition based on EDS map spectra showed that in all the samples, the element contents correspond to the nominal chemical formula of the compound. The EDS image confirms the uniform distribution of Ho atoms over granules.

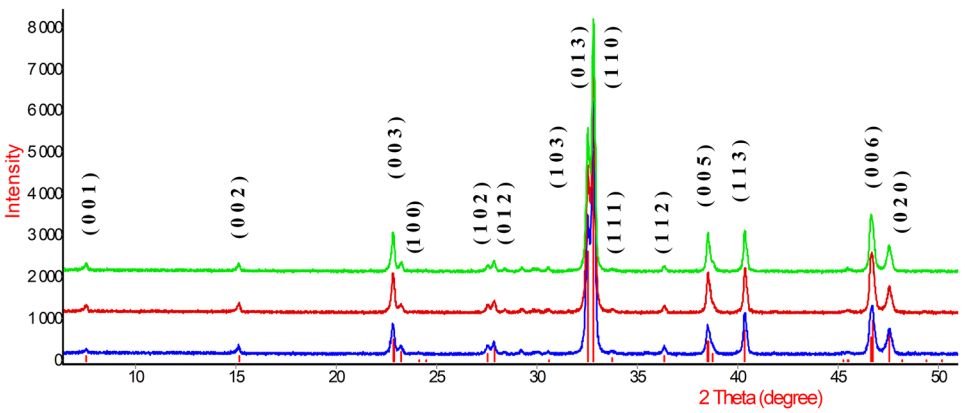

Fig. 1 X-ray diffraction. For clarity, curves are shifted along the intensity axis. Red marks indicate the $YBa_2Cu_3O_{6.96}$ reference

Figure 3 shows the ρ(*T*) dependences of the samples. At temperatures above T_c, these dependences exhibit the metal-like behavior typical of the YBCO system. Different values of resistivity of the samples above T_c are possibly due to occasional microcracks in polycrystalline samples [13]. The sharp resistance drop corresponds to the superconducting transition of granules. The smooth part of the ρ(*T*) dependence is due to the transition in the intergranular subsystem [14, 15]. For all the samples, the temperature width of the smooth part is 3−6 K. We suppose that the substitution of Ho for Y in $Y_{1-x}Ho_xBa_2Cu_3O_{7-\delta}$ almost do not affect the intergranular subsystem in the samples.

Inset of Fig. 3 shows temperature dependences of the magnetic moment *M*(*T*) for #1 and #3 measured under zero field-cooled conditions in a magnetic field of 0.1 T. The superconducting transition temperature T_c determined from temperature dependences of magnetization and resistivity is about 93 K for all the samples.

Figure 4 shows the magnetic hysteresis loops (MHLs) for the $Y_{1-x}Ho_xBa_2Cu_3O_{7-\delta}$ samples in the temperature range of 4.2 – 80 K. The *M*(*H*) dependences are tilted anticlockwise and their tilt increases with the Ho content *x*.

The tilt of the magnetization dependencies emerges apparently due to the paramagnetic magnetization [3, 4, 7]. The experimental MHLs are the sum of a paramagnetic magnetization of Ho ions, $M_P(H)$, and a magnetization of superconducting granules, $M_S(H)$. These subsystems are to be separated for a further analysis.

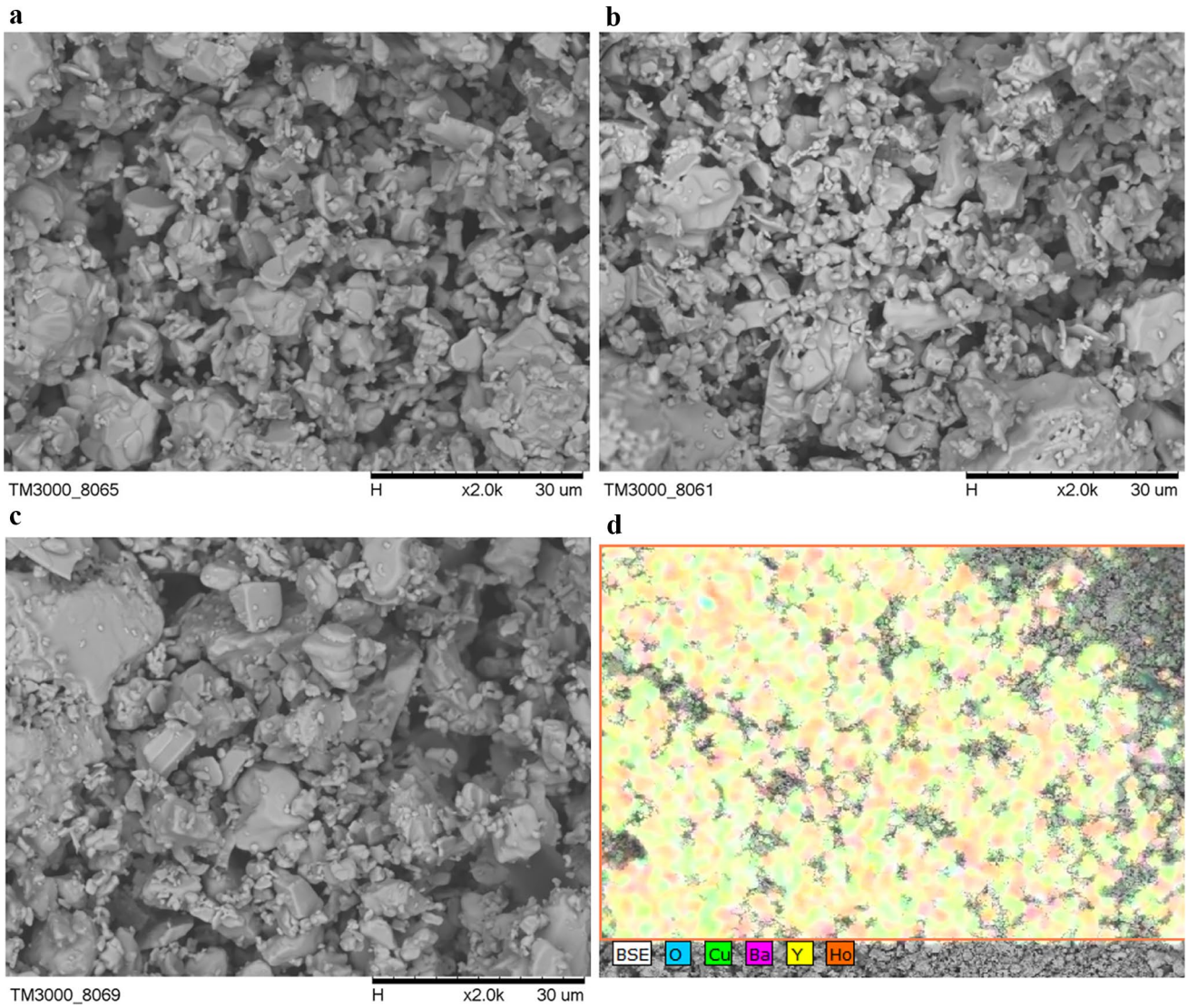

Fig. 2 SEM images of **a** #1, **b** #2, and **c** #3 and **d** EDS image of #3

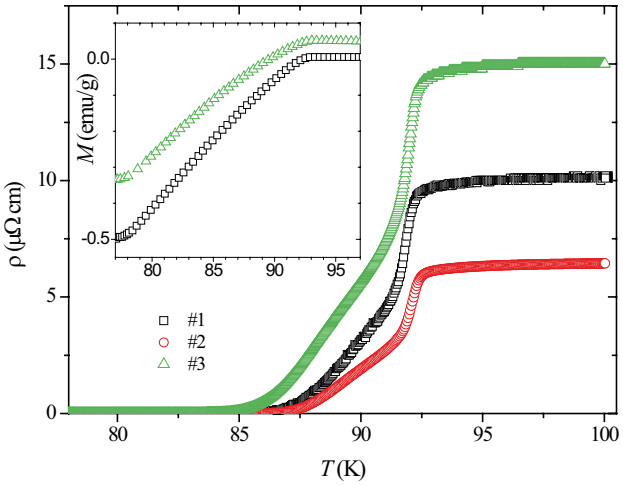

Fig. 3 Temperature dependences of resistivity, $H=0$. Inset: temperature dependences of magnetization, $\mu_0 H=0.1$ T, $T<100$ K

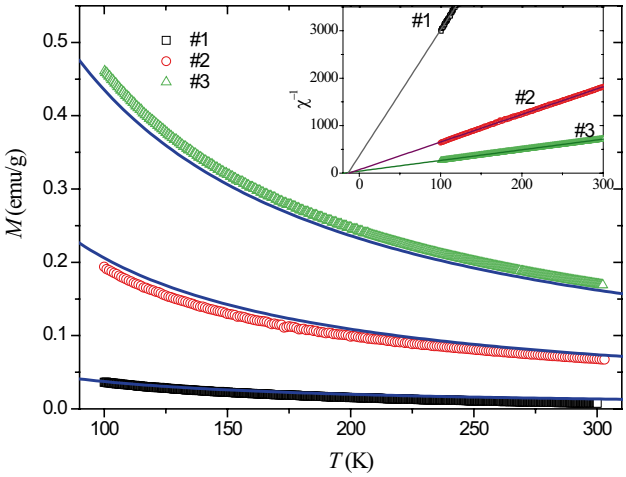

Fig. 5 Magnetization of the samples above 100 K, $\mu_0 H=1$ T. Inset: the inverted susceptibility versus temperature (lines are linear approximations)

4 Analysis

4.1 Paramagnetic Subsystem

Above T_c the magnetization is paramagnetic for all the samples (Fig. 5). The inverted susceptibility $\chi^{-1}=(M/H)^{-1}$ is plotted on inset of Fig. 5. Temperature dependencies $\chi^{-1}(T)$ are linear. The lines on inset of Fig. 5 are described by the relation $\chi=C/(T-\Theta)$, with a Curie–Weiss constant C and a Curie–Weiss temperature Θ. The lines intersect the T axis at −14 K for #1, −12 K for #2, and −19 K for #3. Therefore, Θ is negative for all the samples, indicating antiferromagnetic correlations between Ho ions. The antiferromagnetic coupling was reported earlier for RE based cuprates [3, 16, 17]. In this case, the paramagnetic magnetization is taken into account as

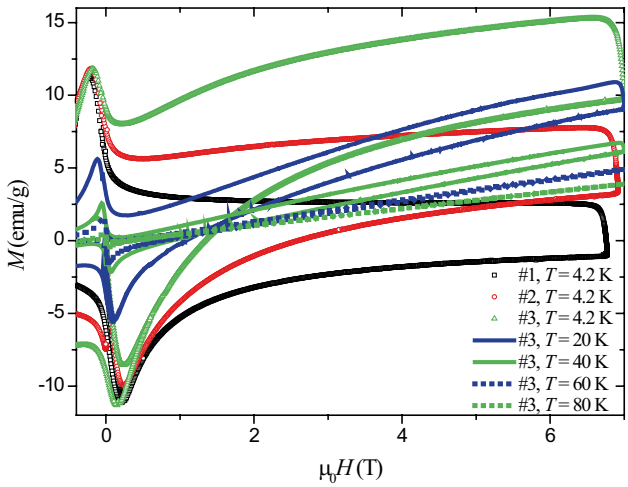

Fig. 4 Magnetic hysteresis loops of studied samples

$$M_P(H,T) = NgJ\mu_B B_J\left(\frac{gJ\mu_B\mu_0 H}{k_B(T-\theta)}\right), \quad (1)$$

where N is the number of magnetic ions per unit volume, μ_B is the Bohr magneton, k_B is the Boltzmann constant, g is the Lande g-factor, J is the angular momentum quantum number, and B_J is the Brillouin function. Solid curves on Fig. 5 are computed by relation (1) with parameters for Ho^{3+} ions ($J=8$ and $g=1.25$), N for the nominal compositions ($x\cdot 5.76\cdot 10^{27}$ m^{-3}), and Θ values from Table 1. Although no fitting parameters were used, agreement between experimental data above 100 K and computed curves is quite good.

The relation (1) was used again to separate the superconducting contribution from the experimental MHLs: $M_S(H)=M(H)-M_P(H)$. The correctness criterion for the separation is zero tilt of resulted superconducting MHLs in high fields H. The limiting of $\Theta<0$, as for the $M(T)$ curves above T_c, does not allow us to plot accurate $M_S(H)$ dependencies. An example of disturbed MHL for $\Theta=-19$ K is presented in Fig. 6. Providing $\Theta=0$, a fitting parameter is required anyway to plot an undisturbed $M_S(H)$ loop. An effective value of N is used to be the fitting parameter. The MHLs without the paramagnetic contribution are plotted on Fig. 6.

Above T_c, all Ho atoms contribute to the magnetization and there are antiferromagnetic correlations between the magnetic ions. Below T_c, the surface superconducting currents screen an inner from the external magnetic field. The concentration of unscreened magnetic ions N_{un} is found to decrease with temperature (inset of Fig. 6). Only the magnetic moments of Ho ions on the surface and in normal cores of the Abrikosov vortices contribute to the paramagnetic magnetization. More than half of Ho atoms are screened

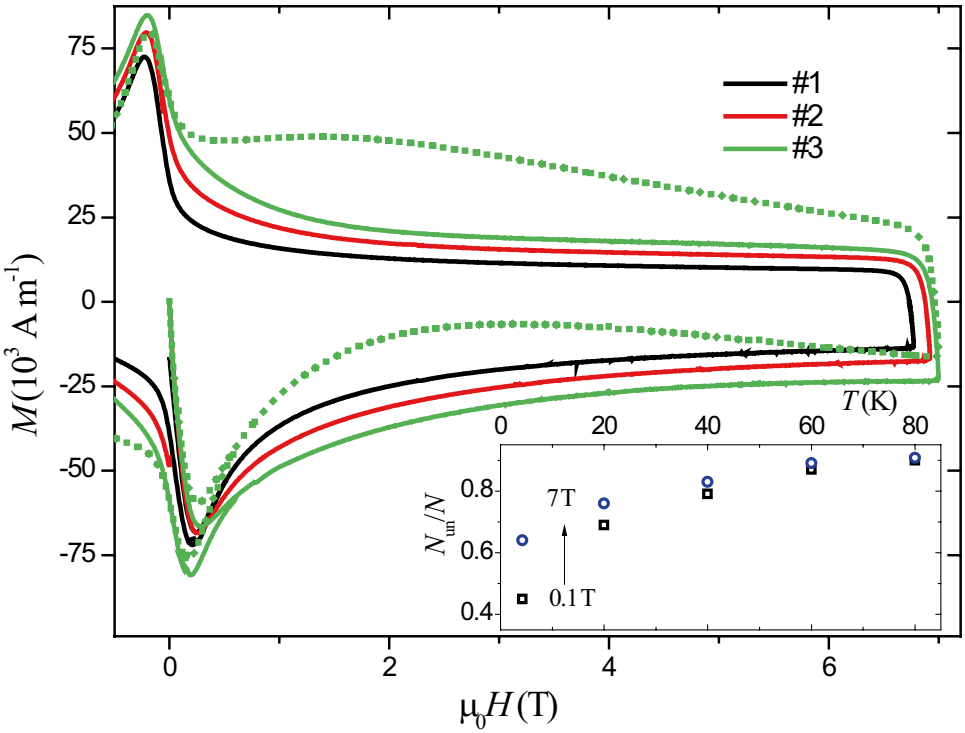

Fig. 6 Magnetic hysteresis loops without paramagnetic contribution at $T=4.2$ K. The dotted curve is disturbed MHL for $\Theta=-19$ K. Inset: the share of unscreened Ho atoms at different temperatures and $\mu_0 H=0.1$ T and 7 T

at $T=4.2$ K. As the temperature increases, both the vortex cores and the surface layer depth expanse so the larger number of Ho atoms become unscreened and contribute to the magnetization. The $\Theta=0$ condition below T_c may mean that antiferromagnetic correlations are blocked in superconducting state. We assume that a modification of electronic spectra during the superconducting transition [18] is a reason of this cutoff.

4.2 Superconducting Subsystem

The Bean formula $J_c=3\Delta M/d$ was used to obtain the critical current density J_c from the experimental MHLs; here, ΔM is the difference between the ascending and descending hysteresis branches and d is the characteristic current circulation size. A change of the theoretical density of $Y_{1-x}Ho_xBa_2Cu_3O_{7-\delta}$ (from 6.38 g/cm^3 for #1 to 6.55 g/cm^3 for #3) was accounted to convert experimental values of the mass magnetization to the volume magnetization. The d value was calculated from an asymmetry of the $M_S(H)$ loops. According to [19], $d \approx 2\lambda_L / [1-0.8|\Delta M/M_{min}|^{1/3}]$, where λ_L is the London penetration depth and M_{min} is the low-field peak magnetization. The circulation size d (Table 1) was found to be about the average granule size obtained from the SEM data. Therefore, the estimated J_c values are the intragranular critical current density. The resulted $J_c(H)$ dependences are presented in Fig. 7a. The $J_c(H)$ dependences for some temperatures demonstrate non-monotonic behavior. They have a flat hump, a second peak. This hump manifests the fishtail feature on MHSs. This fishtail feature is difficult to distinguish on the plotted MHLs (Fig. 4). The related compounds $Y_{1-x}Nd_xBa_2Cu_3O_{7-\delta}$ [7, 10], $Y_{1-x}Gd_xBa_2Cu_3O_{7-\delta}$ [3], and $Y_{1-x}Eu_xBa_2Cu_3O_{7-\delta}$ [11, 20] demonstrate the fishtail feature on MHLs too. The fishtail feature reflects different pinning mechanisms in lower and higher magnetic fields [21, 22]. For YBCO compounds, the peak effect is usually attributed to transitions of the Abrikosov vortex lattice [7, 23, 24]. Due to this transition, the pinning force has a maximum at the related value of the external magnetic field.

The pinning force density F_p is determined by $F_p(H)=\mu_0 H J_c(H)$. The $F_p(H)$ dependences at $T=60$ K are plotted in Fig. 7b. For related polycrystalline $Y_{1-x}RE_xBa_2Cu_3O_{7-\delta}$ compounds, the position of maximum H_{peak} is in 5 times smaller than the irreversibility field $H_{irr}(T)$ [7, 10, 11]. Lines in Fig. 7b are computed with using the Dew-Hughes scaling relation [25] $f_p(h)=h^p(1-h)^q/[h_0^p(1-h_0)^q]$; here, $f_p=F_p(H)/F_{max}(T)$, $h=H/H_{irr}(T)$, $h_0=p/(p+q)$, where $F_{max}(T)$ is the maximum of the $F_p(H)$ dependence. The scaling coefficients $p=1.5$ and $q=6$ were used.

In addition, the maximum field H_{peak} depends on the Ho content x. H_{peak} monotonically decreases as x increases (inset of Fig. 7b). This means that the doping with rare-earth elements reduces characteristic fields of the order–disorder transition in the $Y_{1-x}RE_xBa_2Cu_3O_{7-\delta}$ compound [7, 26]. Therefore, the paramagnetic subsystem influences on the Abrikosov vortex lattice in the superconducting subsystem.

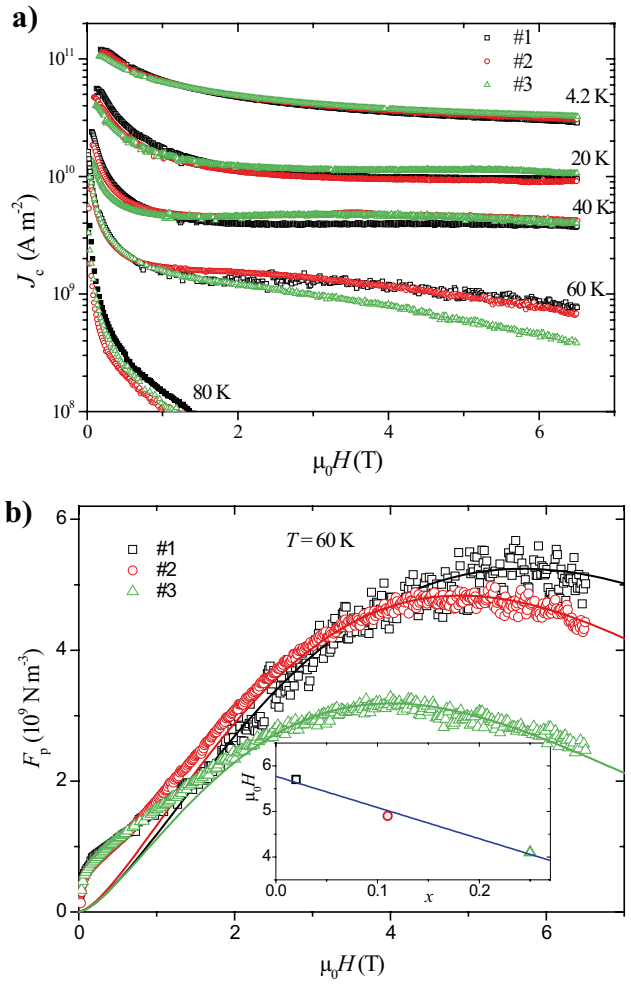

Fig. 7 Magnetic field dependencies of **a** critical current density and **b** pinning force density. Inset of **b**: the peak field versus Ho content (line is a linear approximation)

5 Conclusions

Polycrystalline $Y_{1-x}Ho_xBa_2Cu_3O_{7-\delta}$ ($x = 0.02$, 0.11, and 0.25) superconductors were synthesized and characterized. Two magnetic subsystems are detected in these compounds: the paramagnetic subsystem formed by Ho atoms and the superconducting subsystem residing at a whole sample. The superconducting subsystem veils the paramagnetic atoms and presumably damps antiferromagnetic correlations. The paramagnetic subsystem regulates the phase transition of Abrikosov vortex lattice. It was also found that substitution of Ho for Y does not change the critical current density and the critical temperature.

Acknowledgements We are thankful to M.I. Kolkov, S.V. Komogortsev, A.N. Lavrov, S.N. Martynov, I.V. Nemtsev, and K.A. Shaykhutdinov for useful discussions and to A.V. Shabanov and I.V. Nemtsev for the SEM measurements.

Funding This work was supported by the Russian Foundation for Basic Research and the Government of the Krasnoyarsk Territory, Krasnoyarsk Territorial Foundation for Support of Scientific and R&D Activities, project "Superconducting properties of YBCO incorporated by paramagnetic rare-earth elements" No. 20–42-240008.

References

1. Allgeier, C., Schilling, J.S.: Magnetic susceptibility in the normal state: a tool to optimize Tc within a given superconducting oxide system. Phys. Rev. B. **48**, 9747–9753 (1993). https://doi.org/10.1103/PhysRevB.48.9747
2. Mamsurova, L.G., Trusevich, N.G., Pigalskiy, K.S., Vishnev, A.A., Gadzhimagomedov, S.K., Murlieva, Z.K., Palchaev, D.K., Bugaev, A.S.: Magnetization and static magnetic susceptibility of fine-crystalline high-temperature YBa2Cu3Oy superconductors synthesized by the sol–gel method. Russ. J. Phys. Chem. B. **12**, 908–915 (2018). https://doi.org/10.1134/S1990793118050081
3. Theuss, H., Kronmüller, H.: Magnetic properties of Y1-xGdxBa2Cu3O7-δ polycrystals. Phys. C Supercond. its Appl. **242**, 155–163 (1995). https://doi.org/10.1016/0921-4534(94)02404-9
4. Sandu, V., Popa, S., Di Gioacchino, D., Tripodi, P.: Paramagnetism and superconductivity in Eu0.7Sm0.3Ba2Cu3O7-δ. J. Supercond. Nov. Magn. **17**, 701–710 (2004). https://doi.org/10.1007/s10948-004-0830-8
5. Petrov, M.I., Gokhfeld, Y.S., Balaev, D.A., Popkov, S.I., Dubrovskiy, A.A., Gokhfeld, D.M., Shaykhutdinov, K.A.: Pinning enhancement by heterovalent substitution in Y1-xRExBa2Cu3O7-δ. Supercond. Sci. Technol. **21**, (2008). https://doi.org/10.1088/0953-2048/21/8/085015
6. Öztürk, A., Doğan, M., Düzgün, İ, Çelebi, S.: The effect of Dy doping on the magnetic behavior of YBCO superconductors. J. Supercond. Nov. Magn. **29**, 1787–1791 (2016). https://doi.org/10.1007/s10948-016-3493-3
7. Gokhfeld, D.M., Balaev, D.A., Yakimov, I.S., Petrov, M.I., Semenov, S.V.: Tuning the peak effect in the Y1−xNdxBa2Cu3O7−δ compound. Ceram. Int. **43**, 9985–9991 (2017). https://doi.org/10.1016/J.CERAMINT.2017.05.011
8. Abrikosov, A.A., Gor'kov, L.P.: Contribution to the theory of superconducting alloys with paramagnetic impurities. Sov. Phys. JETP. **12**, 1263 (1961). https://doi.org/10.1142/9789814366960
9. Malik, S.K., Umarji, A.M., Shenoy, G.K.: Depression of the superconducting transition temperature of the Heusler alloy Pd2YSn with the addition of magnetic rare-earth metals. Phys. Rev. B. **32**, 4426–4430 (1985). https://doi.org/10.1103/PhysRevB.32.4426
10. Altin, E., Gokhfeld, D.M., Kurt, F., Yakinci, Z.D.: Physical, electrical, transport and magnetic properties of Nd(Ba,Nd)2.1Cu3O7−δ system. J. Mater. Sci. Mater. Electron. **24**, 5075–5084 (2013). https://doi.org/10.1007/s10854-013-1526-2
11 Altin, E., Gokhfeld, D.M., Demirel, S., Oz, E., Kurt, F., Altin, S., Yakinci, M.E.: Vortex pinning and magnetic peak effect in Eu(Eu, Ba)2.125Cu3Ox. J. Mater. Sci. Mater. Electron. **25**, 1466–1473 (2014). https://doi.org/10.1007/s10854-014-1753-1
12 Petrov, M.I., Balaev, D.A., Gokhfel'd, Y.S., Dubrovskiĭ, A.A., Sha'khutdinov, K.A.: Effect of heterovalent substitution of rare-earth elements on the magnetic and transport properties of YBa2Cu3O7. Phys. Solid State. **49**, 2047–2051 (2007). https://doi.org/10.1134/S1063783407110054
13. Gokhfeld, D.M., Balaev, D.A., Shaykhutdinov, K.A., Popkov, S.I., Petrov, M.I.: Current-voltage characteristics of break junctions of

high-Tc superconductors. Phys. C Supercond. its Appl. **467**, 80–84 (2007). https://doi.org/10.1016/j.physc.2007.09.001
14. Derevyanko, V.V., Sukhareva, T.V., Finkel', V.A.: Effect of the temperature, external magnetic field, and transport current on electrical properties, vortex structure evolution processes, and phase transitions in subsystems of superconducting grains and "weak links" of granular two-level high-temperature superconductor YBa2Cu3O7–δ. Phys. Solid State. **60**, 470–480 (2018). https://doi.org/10.1134/S1063783418030083
15. Semenov, S.V., Balaev, A.D., Balaev, D.A.: Dissipation in granular high-temperature superconductors: new approach to describing the magnetoresistance hysteresis and the resistive transition in external magnetic fields. J. Appl. Phys. **125**, 033903 (2019). https://doi.org/10.1063/1.5066602
16. Lee, B.W., Ferreira, J.M., Dalichaouch, Y., Torikachvili, M.S., Yang, K.N., Maple, M.B.: Long-range magnetic ordering in the high-Tc superconductors RBa2Cu3O7 (R = Nd, Sm, Gd, Dy, and Er). Phys. Rev. B. **37**, 2368–2371 (1988). https://doi.org/10.1103/PhysRevB.37.2368
17. Obradors, X., Visani, P., de la Torre, M.A., Maple, M.B., Tovar, M., Pérez, F., Bordet, P., Chenavas, J., Chateigner, D.: Rare-earth magnetic ordering in the R2CuO4 cuprates (R = Tb, Dy, Ho, Er and Tm). Phys. C Supercond. its Appl. **213**, 81–87 (1993). https://doi.org/10.1016/0921-4534(93)90761-E
18. Bourges, P., Sidis, Y., Fong, H.F., Regnault, L.P., Bossy, J., Ivanov, A., Keimer, B.: The spin excitation spectrum in superconducting YBa2Cu3O6.85. Science (80-.). **288**, 1234–1237 (2000). https://doi.org/10.1126/science.288.5469.1234
19. Gokhfeld, D.M.: The circulation radius and critical current density in type II superconductors. Tech. Phys. Lett. **45**, 1–3 (2019). https://doi.org/10.1134/S1063785019010243
20. Li, Y., Perkins, G.K., Caplin, A.D., Cao, G., Ma, Q., Wei, L., Zhao, Z.X.: Study of the pinning behaviour in yttrium-doped Eu-123 superconductors. Supercond. Sci. Technol. **13**, 1029–1034 (2000). https://doi.org/10.1088/0953-2048/13/7/321
21. Jirsa, M., Pust, L., Dlouhý, D., Koblischka, M.: Fishtail shape in the magnetic hysteresis loop for superconductors: Interplay between different pinning mechanisms. Phys. Rev. B - Condens. Matter Mater. Phys. **55**, 3276–3284 (1997). https://doi.org/10.1103/PhysRevB.55.3276
22. Gokhfeld, D.: Use of a Sigmoid function to describe second peak in magnetization loops. J. Supercond. Nov. Magn. **31**, 1785–1789 (2018). https://doi.org/10.1007/s10948-017-4400-2
23. Koshelev, A.E., Vinokur, V.M.: Pinning-induced transition to disordered vortex phase in layered superconductors. Phys. Rev. B. **57**, 8026–8033 (1998). https://doi.org/10.1103/PhysRevB.57.8026
24. Babich, I.M., Brandt, E.H., Mikitik, G.P., Zeldov, E.: Critical current in type-II superconductors near the order-disorder transition. Phys. Rev. B. **81**, 054517 (2010). https://doi.org/10.1103/PhysRevB.81.054517
25. Dew-Hughes, D.: Flux pinning mechanisms in type II superconductors. Philos. Mag. **30**, 293–305 (1974). https://doi.org/10.1080/14786439808206556
26. Hyun, O.B., Hirabayashi, I.: Effects of local moments on the magnetization of HoBa2Cu3O7. Phys. Rev. B. **50**, 16023–16027 (1994). https://doi.org/10.1103/PhysRevB.50.16023

Publisher's Note Springer Nature remains neutral with regard to jurisdictional claims in published maps and institutional affiliations.